IEEE Access
Multidisciplinary | Rapid Review | Open Access Journal

Received 25 May 2024, accepted 18 June 2024, date of publication 26 June 2024, date of current version 5 July 2024.

Digital Object Identifier 10.1109/ACCESS.2024.3419560

RESEARCH ARTICLE

Design of Wideband Substrate Integrated Waveguide Filters With Tunable Lowpass Characteristics

CLARA MÁXIMO-GUTIÉRREZ[1,2], JUAN HINOJOSA[3], AND ALEJANDRO ALVAREZ-MELCON[1], (Senior Member, IEEE)

[1]Department of Information and Communications Technology, Universidad Politécnica de Cartagena, 30202 Cartagena, Spain
[2]Research Group in Advanced Telecommunications (GRITA), Universidad Católica de Murcia (UCAM), 30107 Guadalupe, Spain
[3]Department of Electronics and Computer Engineering, Universidad Politécnica de Cartagena, 30202 Cartagena, Spain

Corresponding author: Juan Hinojosa (juan.hinojosa@upct.es)

This work was supported by the Agencia Estatal de Investigación (AEI) and Fundación Séneca Region de Murcia of Spain under Grant TED2021-129196B-C42, Grant PID2022-136590OB-42, and Grant 22076/PI/22.

ABSTRACT In this paper, the application of the stepped impedance synthesis technique in the design of tunable wideband substrate integrated waveguide (SIW) Chebyshev filters is explored. By employing Chebyshev transfer functions and stepped impedances, achieved through impedance inverters, a Chebyshev bandpass response can be attained by combining the lowpass characteristics of this stepped impedance technique with the highpass behavior of the SIW (quasi-TE_{10} mode). The novel contribution of this work lies in extending this approach to designing tunable wideband SIW filters using varactor diode tuning elements. Unlike existing design methods of tunable SIW bandpass filters, the proposed technique fixes the lower cut-off frequency of the bandpass response around the cut-off frequency of the SIW TE_{10} mode, while essentially allowing adjustment of the higher cut-off frequency. This adjustment is facilitated by varying the impedance inverters and phase shifts of the filter sections. This is achieved by inserting varactor diodes between elliptic patterns and the SIW structure, and between SIW line sections and floating metallic posts. This innovative method has been applied to a third-order tunable wideband SIW filter. The measurements of the manufactured prototype have offered a significant tuning range (15.3%) with high-performance frequency responses (return loss higher than $RL = 13$ dB and insertion loss lower than $IL = 1$ dB), and a completely different tuning mechanism as compared to previous approaches.

INDEX TERMS Bandpass filter, substrate integrated waveguide (SIW), stepped impedance filter, tunable filter, varactor diode.

I. INTRODUCTION

The constant growth of the number of different standards for multichannel wireless and satellite communication systems, increasingly demands for high-performance microwave filters with tunable frequency responses, compact sizes, and cost-effective manufacturing [1], [2]. Tunable wideband bandpass filters are key elements in high data rate applications [3], [4], as they provide flexibility, adaptability, and spectral efficiency, which is crucial for addressing the dynamic and complex challenges of wideband/ultra-wideband systems.

Among the different technologies such as planar, substrate integrated waveguide (SIW) and rectangular waveguides, SIW has some advantages over others for implementing tunable filtering components [5]. It is a hybrid technology that integrates some characteristics and advantages from both planar and rectangular ones. SIW components usually have lower insertion loss and higher power handling capability than microstrip based designs. They provide a

The associate editor coordinating the review of this manuscript and approving it for publication was Wanchen Yang.

© 2024 The Authors. This work is licensed under a Creative Commons Attribution-NonCommercial-NoDerivatives 4.0 License.
For more information, see https://creativecommons.org/licenses/by-nc-nd/4.0/

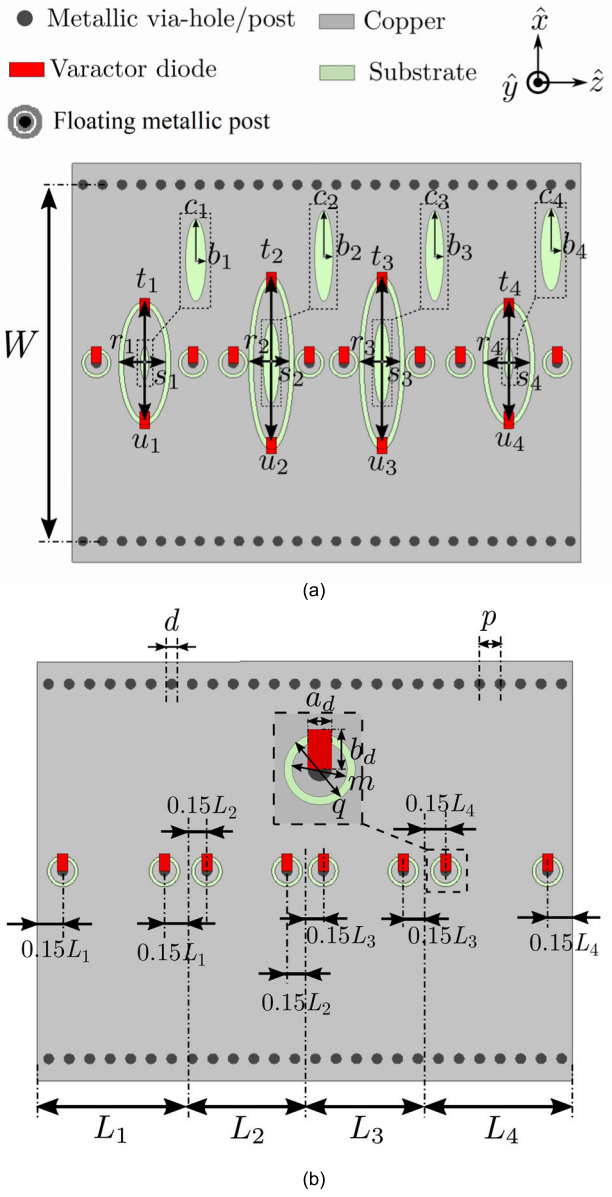

FIGURE 1. Structure of the third-order tunable wideband SIW bandpass filter using varactor diodes (shown as red areas). (a) Top view with insets of the elliptic patterns etched on the metallic ellipses. (b) Bottom view with inset of the floating metallic post.

compact and lightweight solution with a low profile, thus facilitating the integration of active and passive components on the same substrate, unlike those in rectangular waveguides. The manufacturing of SIW components is easier and more cost-effective than their counterparts in rectangular waveguides, since SIW technology is compatible with printed circuit board (PCB) and low-temperature cofired ceramic (LTCC) techniques.

A large number of tuning elements and materials have been used to implement reconfigurable SIW bandpass filters for microwave applications. The implementation of these filters is mainly based on cavities that include tuning through screws [6], ferroelectric ceramics [7], varactor diodes and ferrite slabs [8], thin-film capacitors [9], RF MEMS switches [10], [11], liquid metal [12], varactor diodes [13], [14], [15]; as well as resonators using liquid crystal [16], pin diodes [17], and varactor diodes [18], [19]. Due to their cavity- and resonator-based configurations, these SIW bandpass filters are usually characterized by their narrow bandwidths ($FBW < 10\%$). In these designs, the extensive use of varactor diodes is emphasized, owing to their advantages compared to the other tuning elements and materials. Mainly, the varactor diodes provide a large range of continuous frequency tuning by varying their capacitance, which can change quickly in response to low levels of control signals. In addition, they have a reduced size and weight and are not prone to mechanical wear since they have no moving parts. All these benefits make varactor diodes together with SIW technology attractive for applications that require high-performance components (filters), compact sizes, and easy and cost-effective manufacturing such as in communication systems.

TABLE 1. Design specifications for the tunable wideband SIW bandpass filter.

Parameter	Value
Filter type	Chebyshev
Order n	3
Return loss in the passband, RL (dB)	20
Cut-off frequency of the SIW $f_{c,SIW}$ (GHz)	2.17
Higher cut-off frequency at $\lvert S_{11}\rvert = -20$ dB, $f_{c,H}$ (GHz)	3.45
Cut-off angle, θ_e (°)	25
Substrate permittivity, ε_r	10.2
Thickness of the substrate, h (mm)	0.635

In this paper, the potential of the stepped impedance synthesis technique is applied to the design of tunable wideband SIW filters. The synthesis technique employs Chebyshev transfer functions and impedance inverters [1], [20], which are achieved through appropriately distributed, and dimensioned elliptic patterns along a SIW line. In the same way as [21], it is possible to achieve a bandpass response by combining the lowpass stepped impedance technique with the highpass behavior (quasi-TE_{10} mode) of the SIW. The significant advance presented in this work lies in extending this approach for the first time to the design of third-order tunable wideband SIW filters using varactor diode tuning elements. Unlike the design methods described in [6], [7], [8], [9], [10], [11], [12], [13], [14], [15], [16], [17], [18], and [19], in the proposed method, the lower cut-off frequency ($f_{C,L}$) of the passband varies little and it is close to the cut-off frequency of the SIW TE_{10} mode (f_c (TE_{10})). Only the higher cut-off frequency ($f_{C,H}$) of the passband can be essentially adjusted by acting on the varactors' control signals. To carry out this purpose, the impedance inverters implemented by elliptic patterns and the phase shifts of the SIW sections are varied. This is achieved by placing varactor diodes in parallel between the elliptic patterns and the SIW structure, as well as between the line sections of the SIW and floating metallic

TABLE 2. SIW dimensions for $f_{C,L} = 2.17$ GHz.

Parameter	Value (mm)	Parameter	Value (mm)
d	0.6	p	1.1
W	21.9		

posts that were added to perform phase shift adjustments. Parallel diode connections in these specified locations of the proposed filter provide increased capacity, a decrease in insertion loss due to the lower equivalent resistance, and improved reliability, since one of the diodes can continue to operate in case the other fails.

This paper is organized as follows. The design of a third-order tunable wideband SIW filter is described in Section II. The manufacturing of a prototype and its measurements are presented in Section III. Furthermore, the performance of the proposed filter is compared with other tunable SIW bandpass filters. Finally, conclusions are given in Section IV.

II. DESIGN OF THE TUNABLE WIDEBAND SIW BANDPASS FILTER

The structure of the proposed tunable wideband SIW bandpass filter is shown in Fig. 1. It is a third-order bandpass filter with elliptic patterns, floating metallic posts and varactor diodes. The bandpass response is achieved by combining the highpass behavior of the SIW (quasi-TE_{10} mode) and the lowpass characteristics of the elliptic patterns, which are appropriately distributed throughout the structure. In this design, the elliptic patterns work as impedance inverters, the floating metallic posts form isolated pads, and the varactor diodes allow the filter to be tuned at different higher cutoff frequencies ($f_{c,H}$). The steps to design this filter with the specifications included in Table 1 are described below. The electromagnetic (EM) simulations were carried out by means of a commercial simulator (Ansys Electronics).

A. SIW DESIGN

In this subsection, only the basic structure of the SIW (Fig. 1), without varactor diodes, elliptic patterns and floating metallic posts, is considered. The SIW structure is based on two rows of metallic via-holes with diameter d and pitch length p. Both rows are separated by a width W. A substrate with a dielectric permittivity ε_r and thickness h is inserted between the top and bottom plates. Table 2 includes the dimensions of the SIW for $\varepsilon_r = 10.2$ and $h = 0.635$ mm, which were optimized to achieve the cut-off frequency $f_{C,SIW} = 2.17$ GHz given in Table 1 by means of the following relationship [22]

$$f_{c,SIW}(TE_{10}) = \frac{c}{2\sqrt{\varepsilon_r}\left(W - 1.08\frac{d^2}{p} + 0.1\frac{d^2}{W}\right)} \quad (1)$$

where ε_r and c are the relative permittivity of the substrate and the speed of light in vacuum, respectively. Low leakage loss is obtained when $p < 2d$ and $d < 0.2W$.

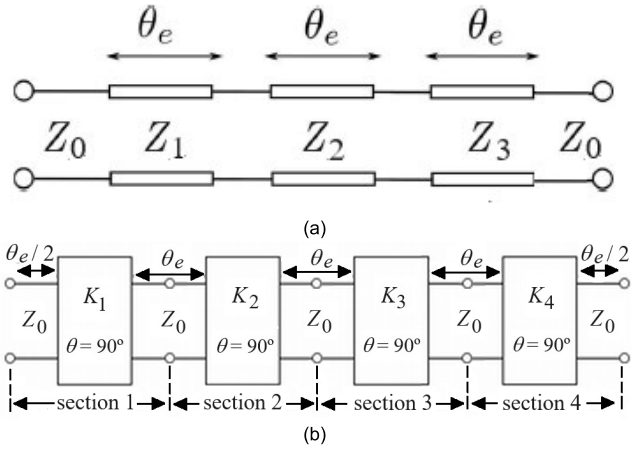

FIGURE 2. Equivalent circuits for a third-order stepped impedance filter. (a) Ideal stepped impedance circuit. (b) Circuit based on impedance inverters.

B. DESIGN OF THE STEPPED IMPEDANCE FILTER

In this subsection, the structure of the third-order bandpass filter (Fig. 1), without varactor diodes, is designed according to specifications included in Table 1. The structure includes four sections of length L_i ($i = 1, \cdots, 4$). Each section is composed of an elliptic pattern and two floating metallic posts centered on the width W of the SIW. As can be seen in Fig. 1, the elliptic patterns are implemented on the top plane of the SIW structure. Each pattern is defined by three ellipses of different sizes inserted between them. The largest and smallest ellipses have, respectively, the dimensions (r_i, t_i) and (b_i, c_i), while those of the intermediate ellipse that is metalized are (s_i, u_i). The metalized intermediate ellipses were added to create isolated pads for connecting the tuning varactor diodes. The floating metallic posts (Fig. 1) have the same dimensions in all four sections of the filter. They are placed at $0.15L_i$ from the input and output of the ith-section. Each floating metallic post is isolated from the top and bottom plates of the filter structure by a circular slot of width $m - q$. The top and bottom circles of diameter m are connected by a metalized via hole to implement the floating metallic posts.

The resulting elliptic pattern acts as impedance inverter and its design parameters together with the length L_i will allow the $S_{ij,i}$ parameters of the ith-section to be adjusted with those values obtained from the synthesis method based on stepped impedances [1], [20]. However, the design of the floating metallic posts should be designed to have little influence on the $S_{ij,i}$ parameters (without varactor diodes) and the filter characteristics.

The bandpass response of the proposed filter is obtained by combining the highpass behavior of the SIW and the lowpass characteristics of the elliptic patterns. The cut-off frequency ($f_{C,SIW}$) of the SIW, indicated in Table 1, was defined in the previous subsection by optimizing the width W of the SIW. The dimensions of the elliptic patterns and length L_i are determined according to the design specifications (Table 1)

TABLE 3. Parameter values extracted from the stepped impedance synthesis method for the equivalent circuits in Fig. 2 and the design specifications given in Table 1.

Parameter	Value (Ω)	Parameter	Value	Parameter	Value
Z_1	2.073	K_1	0.694	$\lvert S_{21,1}\rvert$	0.937
Z_2	0.455	K_2	0.468	$\lvert S_{21,2}\rvert$	0.768
Z_3	02.073	K_3	0.468	$\lvert S_{21,3}\rvert$	0.768
		K_4	0.694	$\lvert S_{21,4}\rvert$	0.937
				$\angle S_{21,i}$, $i = 1, \cdots, 4$	115°

TABLE 4. Dimensions extracted from the design process for the third-order Chebyshev bandpass filter in Fig. 1 and the design specifications given in Table 1.

Parameter	Value (mm)	Parameter	Value (mm)
$L_1 = L_4$	10.3	$L_2 = L_3$	9.2
$r_1 = r_4$	1.16	$r_2 = r_3$	1.46
$s_1 = s_4$	0.96	$s_2 = s_3$	1.17
$t_1 = t_4$	3.8	$t_2 = t_3$	5.23
$u_1 = u_4$	3.46	$u_2 = u_3$	4.9
$b_1 = b_4$	0.25	$b_2 = b_3$	0.5
$c_1 = c_4$	1	$c_2 = c_3$	2.5
q	1.5	m	1

using a synthesis method based on stepped impedances and the following steps [1], [20], [21]:

1) Find the transfer function of the third-order Chebyshev lowpass filter.
2) Extract the three characteristic impedances (Z_i, $i = 1, 2, 3$) of the filter equivalent circuit in Fig. 2(a) using an iterative algorithm between its [ABCD] matrix and the transfer function previously found.
3) Transform the three characteristic impedances (Z_i, $i = 1, 2, 3$) with electrical length θ_e of Fig. 2(a) into the four sections of Fig. 2(b). Each section (Fig. 2(b)) is composed by an impedance inverter (K_i, $i = 1, \cdots 4$) and two SIW lines with the same characteristic impedance Z_0 and electrical length $\theta_e/2$.
4) Find the S_i-parameter of each section of the equivalent circuit depicted in Fig. 2(b).
5) Find the design parameters (L_i, r_i, t_i, b_i, c_i, s_i, u_i) of each section of the filter in Fig. 1, including the floating metallic posts (m, q) and its position ($0.15L_i$), by optimizing the magnitude and phase of its S_i-parameters with those obtained in step 4 using an EM simulator at the higher cut-off frequency ($f_{c,H}$). It is important to remark that the phase adjustment process is able to take into account for the loading effect of the elliptic patterns into the adjacent transmission line sections.
6) Assemble the 4 sections of the filter with the dimensions found in step 5. Perform a final optimization of the filter dimensions to meet the desired specifications (Table 1).

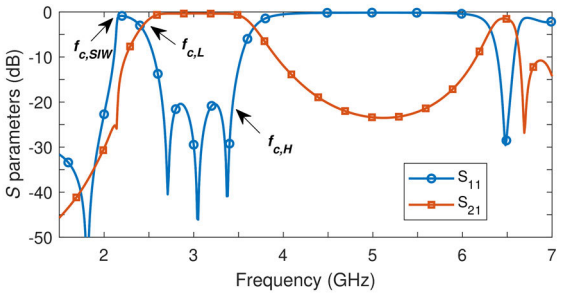

FIGURE 3. Simulated *S*-parameters of the third-order wideband SIW bandpass filter (without varactor diodes).

The values of the normalized impedance inverter and S_i-parameter in steps 3 and 4 are determined by

$$K_i = 1/\sqrt{Z'_{i-1}Z'_i} \tag{2}$$

$$S_{11,i} = S_{22,i} = \frac{K_i/Z_0 - Z_0/K_i}{K_i/Z_0 + Z_0/K_i} e^{-j\theta_e}, \tag{3}$$

$$S_{21,i} = S_{12,i} = \frac{2}{j\,(K_i/Z_0 + Z_0/K_i)} e^{-j\theta_e}, \tag{4}$$

where $i = 1, 2, 3, 4$, $Z'_i = 1/Z_i$ if i is odd or $Z'_i = Z_i$ if i is even, and $Z_0 = 1$.

The values of the parameters extracted from this design process are listed in Tables 3 and 4 for the design specifications indicated in Table 1. Table 3 gives the elements (steps 3 and 4) of the equivalent circuits depicted in Fig 2. The four sections of the circuit shown in Fig. 2(b) have the same phase shift: $\angle S_{21,i} = -90° - \theta_e = -115°$. The physical length L_i of each section of the filter is optimized in step 5 to match $\angle S_{21,i} = -115°$. The final dimensions (step 6) of the third-order Chebyshev bandpass filter shown in Fig. 1 are indicated in Table 4.

Fig. 3 represents the simulated frequency response of the third-order wideband SIW bandpass filter (Fig. 1) after integration of the four individual filter sections, obtained from the previous design process. This frequency response does not include varactor diodes. Filter dimensions are specified in Tables 2 and 4. As can be seen in Fig. 3, the EM simulations coincide with the design specifications (Table 1) and the floating metallic posts have no influence in the frequency range 1.5 GHz – 7 GHz. The lower cut-off frequency $f_{c,L} = 2.4$ GHz of this filter at $|S_{11}| = -3$ dB is essentially due to the highpass behavior of the SIW (quasi-TE_{10} mode). The small difference that can be observed between the lower cut-off frequency of the passband $f_{c,L} = 2.4$ GHz and the cut-off frequency of the SIW $f_c\,(TE_{10}) = 2.17$ GHz is due to a small inductive component introduced by the elliptic pattern as discussed in [23]. In addition, the higher cut-off frequency $f_{c,H} = 3.45$ GHz is consequence of the lowpass characteristics of the four cascaded sections of length L_i with elliptic patterns. The proposed design offers a large 3 dB fractional bandwidth $FBW = 43\%$. The passband presents three reflection zeros and return loss greater than $RL = 20$ dB.

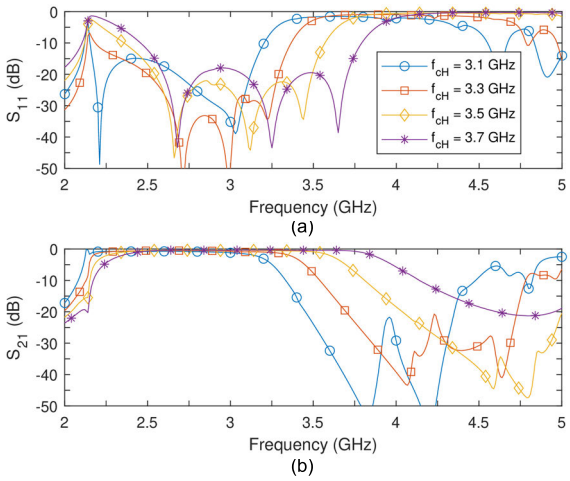

FIGURE 4. Simulated S-parameters of the third-order tunable SIW bandpass filter. (a) $|S_{11}|$. (b) $|S_{21}|$.

TABLE 5. Capacitance values of the varactor diodes required to tune the third-order SIW filter at some frequencies $f_{c,H}$.

$f_{c,H}$ (GHz)	Sections 1 and 4		Sections 2 and 3	
	C_e(pF)	C_f(pF)	C_e(pF)	C_f(pF)
3.1	1.61	0.68	1.39	0.75
3.3	1.24	0.48	1.13	1.02
3.5	0.85	0.47	0.81	1.18
3.7	0.37	0.57	0.48	1.20

where the indices e and f correspond to the varactor diodes connected to the elliptic pattern and floating metallic posts, respectively.

The spurious frequency appears at 6.2 GHz and the maximum rejection level in the stopband reaches $RLSB = 23$ dB. The size of this filter is: 22.5 mm (width) × 39 mm (length) × 0.635 mm (substrate thickness).

C. DESIGN OF THE TUNABLE STEPPED IMPEDANCE FILTER

The objective of this last stage is to add tuning to the higher cutoff frequency ($f_{c,H}$) of the passband to the third-order stepped impedance filter previously designed. For this purpose, silicon abrupt junction varactor diodes SMV1405 from Skyworks MV1405-040LF (packaging: SOD882) have been inserted into the filter as in Fig. 1. This varactor diode exhibits a low series resistance (0.8 Ω), a high Q factor (3200) and a capacitance variation from 0.37 pF to 2.36 pF for reverse voltage between 30 V and 0 V, respectively. As can be seen (Fig. 1), each section of the structure includes six varactor diodes, which have the same dimensions: $a_d \times b_d = 0.6 \times 1\text{mm}^2$. Two of them are located, in parallel, between the top SIW and the x-axis of the elliptic pattern, while the other four are equally placed between the two floating metallic posts and the SIW. Two varactor diodes are mounted in parallel between each floating metallic post and the SIW: one at the top plate and the other one at the bottom plate.

The highpass and lowpass characteristics of the proposed bandpass filter were respectively obtained by adjusting the width W of the SIW and using the design process of the previous subsection based on a stepped impedance technique. Therefore, the structure of the stepped impedance filter was designed according to the equivalent circuit shown in Fig. 2(b). Each section of the filter (Fig. 1) is defined by its length L_i and its elliptic pattern, which respectively perform

TABLE 6. Dimensions of the microstrip-to-SIW transition.

Parameter	Value (mm)	Parameter	Value (mm)
W_m	0.612	L_m	4
L_t	24.9	W_t	7.158
L_{SIW}	5		

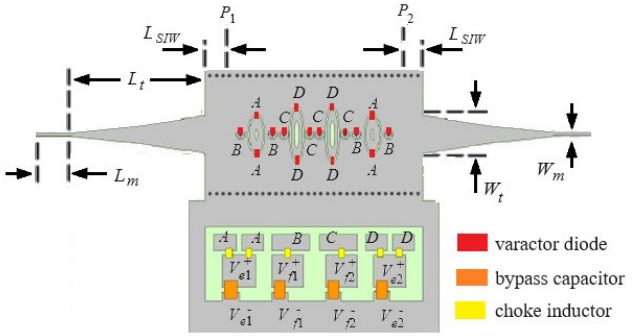

FIGURE 5. Top view of the third-order tunable SIW bandpass filter structure with microstrip-to-SIW transitions and DC bias circuit.

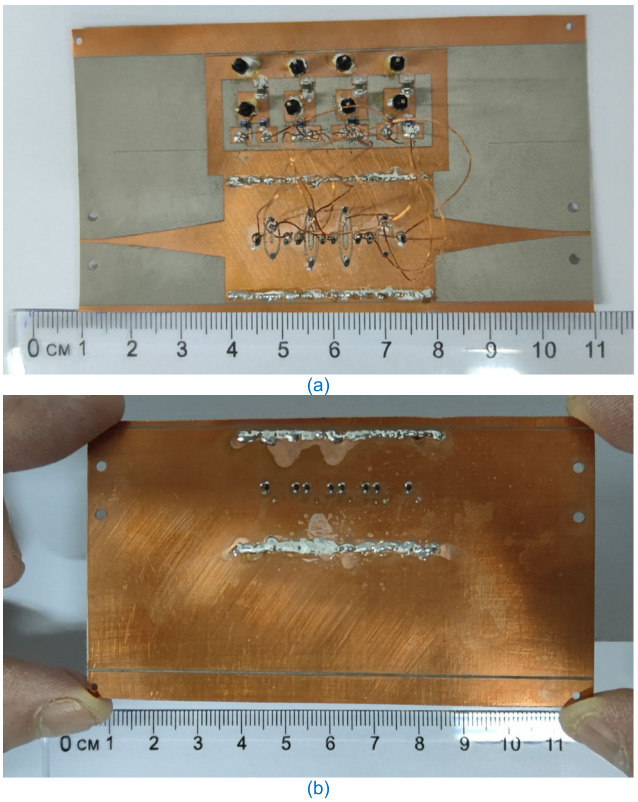

FIGURE 6. Photographs of the manufactured third-order tunable wideband SIW bandpass filter. (a) Top view. (b) Bottom view.

a phase shift $-90 - \theta_e$ and an impedance inverter of value K_i in the equivalent circuit (Fig. 2(b)). In this way, the two varactor diodes placed between the SIW and the elliptic pattern allow K_i to be varied, while the four varactor diodes situated between the SIW and the floating metallic posts are used to adjust θ_e. Parallel diode connections in the impedance inverters (K_i) and in $\theta_e/2$ line sections offer several benefits. The total capacity in these specified locations is increased without raising insertion loss, and the reliability of the filter is improved. Lower insertion loss is due to decreased equivalent resistance when diodes are connected in parallel. Additionally, if one diode fails, the others can continue working, thereby reducing the possibility of a complete filter failure.

The simulated frequency responses of the third-order SIW bandpass filter (Fig. 1) are represented in Fig. 4 for four tuned higher-cutoff frequencies $f_{c,H}$. The capacitance values of the varactor diodes (Skyworks SMV1405), required to tune these frequencies, are indicated in Table 5. As can be seen in Fig. 4, the lower cutoff frequency $f_{c,L}$ varies little around $f_{c,SIW} = 2.17$ GHz, while the higher cutoff frequency $f_{c,H}$ can be adjusted between 3.1 GHz and 3.7 GHz with passband return loss higher than $RL = 15$ dB for all tuned frequencies. The proposed filter offers a tuning range of 17.6% with respect to the tuning center frequency $f_{c,H0} = 3.4$ GHz. The maximum rejection level in the stopband is greater than $RLSB = 20$ dB for the tuning range.

III. FABRICATION AND RESULTS

An exponential microstrip-to-SIW transition has been added at both ports of the filter structure (Fig. 5) [21], with the dimensions indicated in Table 6 for carrying out the measurements. The parameter values for this transition were obtained through electromagnetic simulations and optimization including the filter structure. In addition, a reverse DC bias circuit has also been inserted to control the varactor diodes. The DC bias circuit is based on 6 choke inductors and 4 bypass capacitors to isolate the DC bias from the RF signal, which have the following values $L = 330$ nH (Johanson Technology, ref: LRW0603WJR39GG001E) and $C = 1$ nF (Kyocera AVX, ref: 08055A102JAT2A). Four reverse voltages (V_{e1}, V_{e2}, V_{f1}, V_{f2}) have been needed to tune the proposed bandpass filter. The pads where the positive and negative potentials of these voltages must be applied in the filter structure are indicated in Fig. 5. The connections of the varactor diodes with the four reverse voltages have also been highlighted with the labels A, B, C and D. The designed third-order tunable SIW bandpass filter with the dimensions included in Tables 2, 4 and 6 was manufactured (Fig. 6) using a laser milling machine (LPKF ProtoLaser S) on a RT/Duroid 6010 substrate with the following data: $\varepsilon_r = 10.2$, tg$\delta = 0.0023$ at 10 GHz, substrate thickness $h = 0.635$ mm and copper thickness $t = 18$ μm. An SMA-to-microstrip transition (Southwest) was also added to both filter ports (not shown in Fig. 6) to carry out measurements and coaxial (SMA) connection with the vector network analyzer (VNA, R&S ZVA67). A full two-port TRL calibration of the VNA was previously performed between 2.5 GHz and 6 GHz using a custom SIW TRL kit [24]. Each standard of the custom SIW TRL kit includes microstrip-to-SIW and SMA-to-microstrip transitions. SIW lengths for through, reflect, and line are 10 mm, 5 mm, and 16 mm, respectively. In this way, the reference planes (P_1, P_2) for the measurements of the tunable SIW bandpass filter were located at 5 mm from the input/output ports of the SIW structure (Fig. 5), thus removing unwanted effects from cables, transitions, as well as inherent systematic errors.

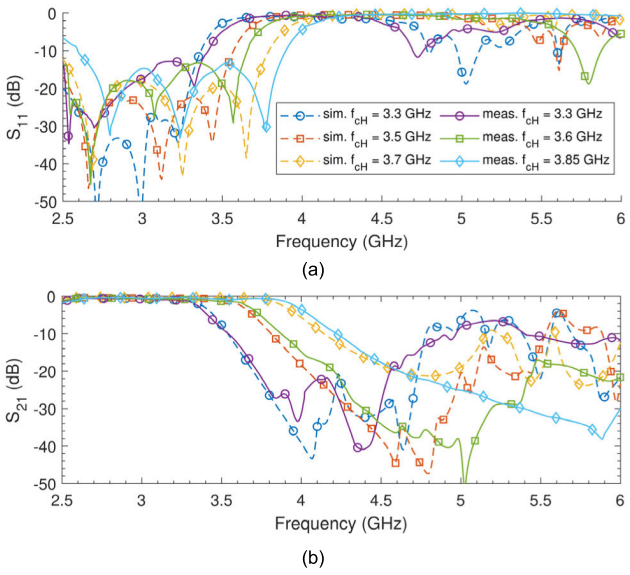

FIGURE 7. Simulated and measured S-parameters of the third-order tunable SIW bandpass filter. (a) $|S_{11}|$. (b) $|S_{21}|$.

Fig. 7 depicts the simulated and measured frequency responses of the manufactured third-order SIW bandpass filter (Fig. 6) for three higher-cutoff frequencies $f_{c,H}$ tuned between their minimum and maximum values. As can be seen, EM simulations and measurements exhibit similar results. The maximum measured higher-cutoff frequency $f_{c,Hm} = 3.85$ GHz shows a slight variation of 0.15 GHz towards a higher frequency with respect to the simulated value $f_{c,Hs} = 3.7$ GHz. This difference is due to possible manufacturing tolerances of the PCB and components, as well as parasitic effects not considered in the EM simulations. The continuous tuning range obtained from measurements is 15.3% with respect to the tuning center frequency $f_{c,H0} = 3.575$ GHz. It is slightly lower than the value (17.6%) achieved for the EM simulated tunable SIW bandpass filter. The measured return and insertion losses in the passband are higher than $RL = 13$ dB and lower than $IL = 1$ dB, respectively. The maximum rejection level in the stopband is higher than $RLSB = 20$ dB for the tuning range.

The measured performance of the proposed third-order tunable SIW bandpass filter is compared in Table 7 with other reconfigurable SIW bandpass filters. As can be seen in this

TABLE 7. Comparison between the proposed tunable SIW bandpass filter and other reconfigurable SIW bandpass filters reported in the literature.

Ref.	Type	Tuning elements*	Order n	Tuning type†	Tuning range in GHz (%)	FBW (%)	RL (dB)	IL (dB)	Q_u	2-D size ($\lambda_0 \times \lambda_0$)
[6] Fig. 5	Resonant cavities	1 screw	1	C	6.85-7.42 (8)	3.5	13	3	94	–
[7] Fig. 7	Resonant cavities	1 FCS + 4 VDs	2	C	2.95-3.57 (19)	5.4	10.9	2.6	60	0.13×0.1
[8] Fig. 17	Resonant cavities	4 FSs + 2 VDs	2	C	10.8-11.86 (9.3)	4	11	1.5	130	0.38×0.63
[9] Fig. 6	Resonant cavities	4 TFCs	2	D (6 states)	1.4/…/2.7 (63.4)	6.2	13	2.7	150	0.24×0.24
[10] Fig. 15	Resonant cavities	6 RF MEMS	2	D (16 states)	1.2/…/1.6 (28.5)	3.7	–	4.1	93	0.41×0.26
[11] Fig. 19	Resonant cavities	2 RF MEMS	2	D (8 states)	0.71/…/1.01 (35.2)	11.4	10	4.2	27	0.06×0.11
[12] Fig. 6	Resonant cavities	LM	2	D (2 states)	1.76/2.02 (13.7)	5.9	16.6	2.6	–	0.7×2.09
[13] Fig.6	Resonant cavities	2 VDs	2	C	2.64-2.88 (8.7)	5.5	20	3.63	–	0.51×0.25
[14] Figs. 2-3	Resonant cavities	2 VDs	1	C	1.91-2.09 (8.9)	7.5	14.8	1.87	–	–
[15] Fig. 15(b)	Resonant cavities	4 PAs+ 6 VDs	3	C	2.47-3.08 (22)	5	10	2.67	–	0.42×0.4
[16] Fig. 13	Resonators	LC	2	C	16.41-17.06 (3.8)	3.9	10	3.4	–	1.8×3.8
[17] Fig. 14	Resonators	2 PDs	1	D (2 states)	5.8/6.8 (15.8)	7	32	0.5	–	0.16×0.25
[18] Fig. 8(b)	Resonators	32 VDs	3	C	1.24-1.8 (36.8)	5	15	4	103	0.6×0.21
[19] Fig. 14(a)	Resonators	4 VDs	2	C	2.34-3 (24.7)	3	12	6.4	–	0.6×0.21
This work	Stepped impedances	24 VDs	3	C	3.3-3.85 (15.3)	43	13	1	12	0.27×0.46

FBW, RL, IL, Q_u and λ_0 are the fractional bandwidth, return loss, insertion loss, unloaded quality factor and free-space wavelength at the center frequency of the tuning range, respectively.
*FCS, FSs, LC, LM, PA, PDs, TFCs and VDs define ferroelectric ceramic substrate, ferrite slabs, liquid crystal, liquid metal, piezoelectric actuators, pin diodes, thin-film capacitors, and varactor diodes, respectively.
†C and D express continuous and discrete tuning ranges, respectively.

comparison table, resonant cavities and varactor diodes are mainly used to design tunable bandpass filters. The order n of these filters varies between 1 and 4. The tuning range is mainly continuous, except for five cases [9], [10], [11], [12], [17]. Discrete tuning designs provide a range between 13.7% and 63.4%, while continuous ones offer a variation between 8% and 36.8%, with the proposed filter being 15.3%. Although filter designs with discrete tuning offer a larger range than their continuous counterparts, they may have some limitations in terms of tuning accuracy and flexibility to adapt to frequency changes compared to those with continuous tuning systems. The tunable SIW bandpass filters are narrowband ($FBW < 10$ %), except [11] and the proposed tunable stepped impedance filter. The implementation of wideband filters based on cavities as in [11] implies increased design and manufacturing complexity due to its folded ridged structure, a limited order, additional losses, and coupling problems in contrast to the proposed SIW filter. Contrary to other design methods that control the center frequency by changing the capacitors of the resonant cavities or resonators, the proposed tunable design technique essentially varies the higher cutoff frequency ($f_{c,H}$). The measured tunable SIW bandpass prototype (Fig. 7) exhibits higher passband performance ($RL = 13$ dB, $IL = 1$ dB) compared to the other filters of order higher than 1. The unloaded quality factor $Q_u = 12$ of the proposed filter, designed from a lowpass prototype according to the design specification in Table 1, has been obtained from the following relationship [20], [25], [26]

$$Q_u = \frac{4.343}{IL} \sum_{i=1}^{n} g_i \tag{5}$$

where $n = 3$, $IL = 1$ dB, and g_i are, respectively, the order of the filter, insertion loss and element values of the lowpass prototype for a passband ripple of 0.043 dB ($RL = 20$ dB): $g_1 = g_3 = 0.8516$, $g_2 = 1.1032$.

Although the insertion loss of the proposed filter is lower compared to the other bandpass filters, except for [17], this is the unloaded quality factor (Q_u) is not higher. This is because the proposed filter has been designed from a lowpass prototype, and bandpass filters have higher Q_u factor due to their narrower bandwidth, leading to higher stored energy in the resonators. The Q_u factor of bandpass filters can be determined using (6) and the fractional bandwidth (FBW) as follows [25], [26]

$$Q_u = \frac{4.343}{FBW \times IL} \sum_{i=1}^{n} g_i \tag{6}$$

These relations indicate that the low insertion loss achieved in our filter is also due to the wideband response, since wideband filters naturally exhibit lower insertion losses than narrowband filters. The normalized size of the proposed filter to a first-order prototype is $0.27\lambda_0 \times 0.153\lambda_0 = 41.4 \times 10^{-3}\lambda_0^2$. This area is 17.6 and 12.5 times smaller and larger than the largest [12] and smallest [11] previously reported tunable SIW bandpass filter, respectively.

In term of cost, the proposed filter was fabricated on a low-cost substrate (RT/duroid 6010) using a conventional PCB process and employs 24 varactor diodes (Skyworks SMV1405-040LF), which are commercially available. Among the tunable filters using varactor diodes listed in Table 7, only one includes a larger number of diodes [18]. Filters that only employ varactor diodes offer a favorable balance between cost, dynamic tuning, and ease of manufacturing compared to those using other tuning elements (screws, ferroelectric substrate, ferrite, liquid crystal, etc.). This makes them a suitable option for applications that require fast and accurate adjustments.

IV. CONCLUSION

This paper has investigated the application of the stepped synthesis technique to design tunable wideband substrate integrated waveguide (SIW) filters. The synthesis method uses Chebyshev transfer functions and impedance inverters, achieved through adequately distributed elliptic patterns along a SIW line. Building upon previous work, where a bandpass response was attained by combining lowpass stepped impedance method with the highpass behavior of SIW, this study extends the approach to develop a third-order tunable wideband SIW filter using varactor diodes as tuning elements. Unlike existing tunable methods, the proposed design essentially fixes the lower cut-off frequency in the passband, being close to the cut-off frequency of the SIW TE_{10} mode, while allowing the higher cut-off frequency to be properly adjusted. This tuning is achieved by varying impedances inverters and phase shifts of the SIW line sections by means of varactor diodes placed in specific locations in the SIW filter structure. The impedance inverters are changed by actuating on the varactor diodes situated between elliptic patterns and the SIW structure, while the phases are shifted through varactor diodes placed between SIW line sections and floating metallic posts. This work, supported by measurements from a manufactured prototype, has marked a significant advancement in the design of tunable wideband SIW filters, thus offering new possibilities for versatile and efficient signal processing applications.

REFERENCES

[1] R. J. Cameron, C. M. Kudsia, and R. Mansour, *Microwave Filters for Communication Systems: Fundamentals, Design, and Applications*. Hoboken, NJ, USA: Wiley, 2018.

[2] E. Laplanche, N. Delhote, A. Perigaud, O. Tantot, S. Verdeyme, S. Bila, D. Pacaud, and L. Carpentier, "Tunable filtering devices in satellite payloads," *IEEE Microwave Mag.*, vol. 21, pp. 69–83, Feb. 2020.

[3] J.-S. Hong, "Reconfigurable planar filters," *IEEE Microwave Mag.*, vol. 10, no. 6, pp. 73–83, Oct. 2009.

[4] R. P. Verma and B. Sahu, "Structure and performance comparison of ultra-wideband bandpass filter: Review article," in *Proc. 7th Int. Conf. Signal Process. Commun. (ICSC)*, Nov. 2021, pp. 118–123.

[5] M. Bozzi, A. Georgiadis, and K. Wu, "Review of substrate-integrated waveguide circuits and antennas," *IET Microwave, Antennas Propag.*, vol. 5, no. 8, p. 909, 2011.

[6] F. Mira, J. Mateu, and C. Collado, "Mechanical tuning of substrate integrated waveguide resonators," *IEEE Microwave Wireless Compon. Lett.*, vol. 22, no. 9, pp. 447–449, Sep. 2012.

[7] Y. Zheng, M. Sazegar, H. Maune, X. Zhou, J. R. Binder, and R. Jakoby, "Compact substrate integrated waveguide tunable filter based on ferroelectric ceramics," *IEEE Microwave Wireless Compon. Lett.*, vol. 21, no. 9, pp. 477–479, Sep. 2011.

[8] S. Adhikari, A. Ghiotto, and K. Wu, "Simultaneous electric and magnetic two-dimensionally tuned parameter-agile SIW devices," *IEEE Trans. Microwave Theory Techn.*, vol. 61, no. 1, pp. 423–435, Jan. 2013.

[9] D. Psychogiou and R. Gómez-García, "Multi-mode-cavity-resonator-based bandpass filters with multiple levels of transfer-function adaptivity," *IEEE Access*, vol. 7, pp. 24759–24765, 2019.

[10] V. Sekar, M. Armendariz, and K. Entesari, "A 1.2–1.6-GHz substrate-integrated-waveguide RF MEMS tunable filter," *IEEE Trans. Microwave Theory Techn.*, vol. 59, no. 4, pp. 866–876, Apr. 2011.

[11] T. R. Jones and M. Daneshmand, "Miniaturized folded ridged quarter-mode substrate integrated waveguide RF MEMS tunable bandpass filter," *IEEE Access*, vol. 8, pp. 115837–115847, 2020.

[12] Y. Mei, B. Liu, Y. Yi, H. Xu, and Y. Zhang, "Liquid metal frequency-reconfigurable SIW bandpass filter based on gravity field," *Electron. Lett.*, vol. 57, no. 12, pp. 481–482, Jun. 2021.

[13] S. Sirci, J. D. Martinez, M. Taroncher, and V. E. Boria, "Analog tuning of compact varactor-loaded combline filters in substrate integrated waveguide," in *Proc. 42nd Eur. Microwave Conf.*, 2013, pp. 257–260.

[14] W. Y. Sam, Z. Zakaria, and M. A. Mutalib, "The investigation of reconfigurable SIW filter using varactor diodes," in *Proc. IEEE 5th Asia–Pacific Conf. Antennas Propag. (APCAP)*, Jul. 2016, pp. 167–168.

[15] J. Lai, T. Yang, P.-L. Chi, and R. Xu, "Novel evanescent-mode cavity filter with reconfigurable rat-race coupler, quadrature coupler and multi-pole filtering functions," *IEEE Access*, vol. 8, pp. 32688–32697, 2020.

[16] D. Jiang, Y. Liu, X. Li, G. Wang, and Z. Zheng, "Tunable microwave bandpass filters with complementary split ring resonator and liquid crystal materials," *IEEE Access*, vol. 7, pp. 126265–126272, 2019.

[17] H. Boubakar, M. Abri, and M. Benaissa, "Design of complementary hexagonal metamaterial based HMSIW band-pass filter and reconfigurable SIW filter using PIN diodes," *Adv. Electromagn.*, vol. 10, no. 2, pp. 19–26, Jul. 2021.

[18] M. Deng and D. Psychogiou, "Tune-all substrate-integrated-waveguide (SIW) bandpass filters," in *Proc. 14th Eur. Microwave Integr. Circuits Conf.*, Paris, France, Sep. 2019, pp. 322–325.

[19] T.-H. Lee, J.-J. Laurin, and K. Wu, "Reconfigurable filter for bandpass-to-absorptive bandstop responses," *IEEE Access*, vol. 8, pp. 6484–6495, 2020.

[20] G. Matthaei, E. M. T. Jones, and L. Young, *Microwave Filters, Impedance-Matching Networks, and Coupling Structures*. Norwood, MA, USA: Artech House, 1980.

[21] C. Máximo-Gutiérrez, J. Hinojosa, and A. Alvarez-Melcon, "Design of wide band-pass substrate integrated waveguide (SIW) filters based on stepped impedances," *Int. J. Electron. Commun.*, vol. 100, pp. 1–8, Feb. 2019.

[22] F. Xu and K. Wu, "Guided-wave and leakage characteristics of substrate integrated waveguide," *IEEE Trans. Microwave Theory Techn.*, vol. 53, no. 1, pp. 66–73, Jan. 2005.

[23] C. Máximo-Gutiérrez, J. Hinojosa, and A. Alvarez-Melcon, "A technique for the passband and stopband control of wideband band-pass substrate integrated waveguide (SIW) filters designed with elliptic stepped impedances," *Int. J. Electron. Commun.*, vol. 177, pp. 155172–155181, Apr. 2024.

[24] E. D. Caballero, A. Belenguer, H. Esteban, and V. E. Boria, "Thru-reflect-line calibration for substrate integrated waveguide devices with tapered microstrip transitions," *Electron. Lett.*, vol. 49, no. 2, pp. 132–133, Jan. 2013.

[25] S. B. Cohn, "Dissipation loss in multiple-coupled-resonator filters," *Proc. IRE*, vol. 47, no. 8, pp. 1342–1348, Aug. 1959.

[26] J. S. Hong and M. J. Lancaster, *Microstrip Filters for RF/Microwave Applications*. Hoboken, NJ, USA: Wiley, 2001.

CLARA MÁXIMO-GUTIÉRREZ was born in Murcia, Spain, in 1993. She received the degree in telecommunication systems, the master's degree in telecommunication engineering, and the Ph.D. degree in information and communication technologies from the Universidad Politécnica de Cartagena (UPCT), Cartagena, Spain, in 2015, 2017, and 2022, respectively.

In 2017, she joined the Department of Information Technologies and Communications, UPCT, as a Research Student, where she was developing her teaching and research activities. Her research interest includes the development of fixed and tunable filters for RF front-end stages in satellite systems. Her research is being carried out in gap waveguide, planar, and multilayer technologies.

JUAN HINOJOSA was born in Dunkerque, France, in 1965. He received the Diplôme d'Etudes Approfondies (D.E.A.) and Ph.D. degrees in electronics from the Université des Sciences et Technologies de Lille (USTL), Lille, France, in 1990 and 1995, respectively.

In 1990, he joined the Hyper-Frequency and Semiconductor Department, Nanotechnologies and Microelectronics, Electronics Institute (IEMN), as a Research Student, where he was involved in the development of electromagnetic characterization techniques of materials at microwave frequencies. Since 1999, he has been developing his teaching and research activities with the Universidad Politécnica de Cartagena, Cartagena, Spain. His research interests include characterization techniques of materials in microwave frequency range, development of novel microwave devices, and modeling techniques for the design of microwave devices.

ALEJANDRO ALVAREZ-MELCON (Senior Member, IEEE) was born in Madrid, Spain, in 1965. He received the Telecommunications Engineer degree from the Technical University of Madrid (UPM), Madrid, Spain, in 1991, and the Ph.D. degree in electrical engineering from the Swiss Federal Institute of Technology, Lausanne, Switzerland, in 1998.

In 1988, he joined the Signal, Systems and Radiocommunications Department, UPM, as a Research Student, where he was involved in the design, testing, and measurement of broad-band spiral antennas for electromagnetic measurements support (EMS) equipment. From 1991 to 1993, he was with the Radio Frequency Systems Division, European Space Agency (ESA/ESTEC), Noordwijk, The Netherlands, where he was involved in the development of analytical and numerical tools for the study of waveguide discontinuities, planar transmission lines, and microwave filters. From 1993 to 1995, he was with the Space Division, Industry Alcatel Espacio, Madrid, and ESA, where he collaborated in several ESA/European Space Research and Technology Centre (ESTEC) contracts. From 1995 to 1999, he was with the Swiss Federal Institute of Technology, École Polytechnique Fédérale de Lausanne, Lausanne, where he was involved with the field of microstrip antennas and printed circuits for space applications. In 2000, he joined the Universidad Politécnica de Cartagena, Spain, where he is currently developing his teaching and research activities.

Dr. Alvarez-Melcon was a recipient of the *Journée Internationales de Nice Sur les Antennes* (JINA) Best Paper Award for the best contribution to the JINA'98 International Symposium on Antennas and the Colegio Oficial de Ingenieros de Telecomunicación (COIT/AEIT) Award to the Best Ph.D. Dissertation in basic information and communication technologies.